sschi SLOVAK SOCIETY OF CHEMICAL ENGINEERING

Slovak Society of Chemical Engineering
Institute of Chemical and Environmental Engineering
Slovak University of Technology in Bratislava

PROCEEDINGS

52nd International Conference of the Slovak Society of Chemical Engineering SSCHE 2026

Hotel SOREA TRIGAN
Štrbské Pleso, Slovakia
May 26 - 29, 2026

Editors: Assoc. prof. Mário Mihaľ

ISBN: 978-80-8208-177-3, EAN: 9788082081773

Published by the Faculty of Chemical and Food Technology, Slovak University of Technology in Bratislava in Slovak Chemistry Library for the Institute of Chemical and Environmental Engineering; Radlinského 9, 812 37 Bratislava, 2026

Sklenář, A., Sauer, L., Přibyl, M.: Free-Flow Electrophoresis: An experimental platform for continuous separation of enantiomers, Editors: Mihaľ, M., In *52nd International Conference of the Slovak Society of Chemical Engineering SSCHE 2026*, Štrbské Pleso, Slovakia, 2026.

Free-Flow Electrophoresis: An experimental platform for continuous separation of enantiomers

Adam Sklenář[1], Lukáš Sauer[1], Michal Přibyl[1,*]
[1]Department of Chemical Engineering, University of Chemistry and Technology, Prague, Technická 5, 166 28 Prague 6, Czech Republic
*Corresponding author: Michal Přibyl, e-mail: pribylm@vscht.cz, tel.: +420 220 444 445

Optically active compounds are widely used as active pharmaceutical ingredients (APIs) or as precursors in drug manufacturing. Therefore, the pharmaceutical industry places strong emphasis on the production of optically pure and enantiomerically enriched compounds. Traditionally, these are obtained through asymmetric synthesis or chromatographic methods, which are often time-consuming, expensive, and unsuitable for continuous operation. Alternatives include enantioselective enzymatic reactions catalyzed by lipases in packed-bed reactors or the separation of enantiomers from racemic mixtures using orthogonal techniques.

Microfluidic technologies and orthogonal separation methods, particularly free-flow electrophoresis (FFE), represent promising approaches for continuous separations. FFE enables fractionation of electrically charged compounds based on differences in electrophoretic mobility. However, its broader application is still limited by lower separation efficiency compared to conventional techniques such as chromatography. Further development therefore requires a deeper understanding of transport phenomena, including interactions between analytes, electrolyte components, and the applied electric field.

In this work, we focused on the separation of mandelic acid enantiomers using a chiral selector dissolved in the electrolyte. A positively charged β-cyclodextrin derivative was used, which preferentially binds to one enantiomer and alters its electrophoretic mobility. Partial enantiomer separation was experimentally demonstrated, indicating the potential of FFE for continuous separation of optically active compounds.

Building on these results, we further develop a concept employing superparamagnetic iron oxide nanoparticles (SPIONs) as mobile carriers of chiral selectors. The nanoparticle surface can be chemically modified to control both ligand attachment and surface charge. Functionalized particles are deflected in the electric field to intersect the racemic stream, enabling selective binding of one enantiomer and its diversion into a different trajectory, while the other continues unaffected. This controlled trajectory crossing represents a promising strategy to enhance the efficiency of continuous enantioseparation in FFE systems.

Publications:

Sklenář, A., Sauer, L., Fialová, L., Řezanka, P., & Přibyl, M. (2025). Transport fundamentals of continuous separation of enantiomers by lateral free-flow electrophoresis in the presence of chiral selectors: experiments and modeling. Separation and Purification Technology, 135468.

Separation and Purification Technology 380 (2026) 135468

Contents lists available at ScienceDirect

Separation and Purification Technology

journal homepage: www.elsevier.com/locate/seppur

Transport fundamentals of continuous separation of enantiomers by lateral free-flow electrophoresis in the presence of chiral selectors: experiments and modeling

Adam Sklenář [a], Kateřina Zedníčková [a], Lukáš Sauer [a], Lada Fialová [b], Pavel Řezanka [b], Michal Přibyl [a,*]

[a] Department of Chemical Engineering, University of Chemistry and Technology, Prague, Technická 5, CZ-166 28 Praha 6, Czech Republic
[b] Department of Analytical Chemistry, University of Chemistry and Technology, Prague, Technická 5, CZ-166 28 Praha 6, Czech Republic

ARTICLE INFO

Keywords:
Free-flow electrophoresis
Capillary electrophoresis
Cyclodextrin
Enantiomers
Continuous-flow separation
Mathematical model

ABSTRACT

Lateral free-flow electrophoresis (FFE) is a potentially powerful technique for the continuous separation of enantiomers. However, the use of FFE is not yet widespread due to its generally lower reliability compared to conventional discontinuous techniques. A key step toward the potential expansion of FFE is a thorough understanding of the fundamental transport mechanisms, particularly the interactions of the separated analytes with other electrolyte components and the applied electric field. To investigate these interactions, we selected a model system comprising mandelic acid and a β-cyclodextrin derivative as the chiral selector. The selector was chosen based on an extensive preliminary study using capillary electrophoresis, which identified it as the most effective for enantioselective binding. Using mathematical models of an orthogonal FFE device, we show a parametric window where the enantiomers of mandelic acid are separable. We revealed the crucial effect of the concentration of a carrier electrolyte on the separation properties of the FFE device. If the concentration of mandelic acid is higher than that of the carrier electrolyte, we observe significant deviations from an ideal behavior predicted by a simple trajectory analysis. Good agreement of the results of experiments and mathematical modeling allowed us to explain this behavior based on understanding the transport fundamentals that are similar to those we observe in system at ion-exchange membranes. Our findings are generalizable to all selector-analyte pairs in which at least one molecule is present in the ionic form, and may thus contribute to the development of continuous separation methods for enantiomers.

1. Introduction

Most low molecular weight drugs are optically active compounds [1], which are, however, often used in the form of racemates. A typical example is ibuprofen, where (*S*)-ibuprofen exhibits anti-inflammatory effects, while (*R*)-ibuprofen is inactive [2] and contributes to the overall burden on the body after drug administration. Active pharmaceutical ingredients as well as various proteins become synthesized continuously in milli- and micro-scale chemical factories [3–5]. Continuous separation of enantiomers from racemic mixtures is therefore crucial for the fully continuous production of a single enantiomer. Applicable continuous separation techniques include, for example, membrane processes with immobilized chiral selectors [6] or orthogonal electroseparation techniques. These include free-flow electrophoresis (FFE) [7], isoelectric focusing [8], isotachophoresis [9], electrochromatography [10].

The principle of free-flow electrophoresis (FFE) is based on the orthogonal arrangement of the velocity and electric fields within the separation chamber. A solution containing the chemicals to be separated is continuously introduced into the carrier electrolyte. These chemicals are transported by the flowing electrolyte while simultaneously being forced by an electric field applied in a perpendicular direction [11]. Based on the different electrophoretic mobilities of the components, the individual chemicals can be deflected from the main flow direction of the electrolyte, forming distinct concentration trajectories. Fractions of the carrier electrolyte containing different amounts of separated components can then be continuously collected from the outlets. Since enantiomers in a racemic mixture possess identical electrophoretic mobilities, the conventional FFE method must be modified. A chiral

* Corresponding author.
E-mail address: pribylm@vscht.cz (M. Přibyl).

https://doi.org/10.1016/j.seppur.2025.135468
Received 19 August 2025; Received in revised form 18 September 2025; Accepted 30 September 2025
Available online 1 October 2025

selector, which preferentially binds to one of the enantiomers, can be introduced into the system along with the racemic mixture. The resulting enantiomer – selector complex exhibits a different electrophoretic mobility due to changes in the molecular weight [9] or net charge [7]. Instead of a soluble selector, a chiral selector immobilized on a stationary phase may be in the orthogonal electrochromatography [12] or in other potentially continuous electrochromatography techniques [13]. The FFE method has already been applied for the separation of enantiomers of piperoxan [7], dansyl phenylalanine [14], methadone [9], tryptophan [8,15], methylphenidate [16], and terbutaline [17] from racemic mixtures. As chiral selectors, charged [7,16,17] or uncharged β-cyclodextrins [9,14] were most commonly employed, along with α-cyclodextrin [15] and human serum albumin [8]. In the majority of the conducted studies, only relatively low enantiomeric excess was achieved [7–9]. Almost complete enantiomeric separation was observed solely when using the Octopus FFE system [14,17].

Compared to other continuous and semi-continuous enantioseparation techniques such as preferential crystallization [18], membrane-based resolution [19], and true moving bed (TMB) chromatography and simulated moving bed (SMB) chromatography [20], FFE offers a unique advantage in its ability to operate without a solid stationary phase and to separate analytes based on dynamic changes in electrophoretic mobility induced by chiral selectors. While membrane and chromatographic methods often rely on immobilized selectors and require complex regeneration protocols, FFE enables selector reuse and real-time adjustment of separation conditions, making it a promising alternative for integration into continuous production systems [21].

In industrial practice, enantiomer separation is typically carried out using TMB and SMB chromatography methods, for which scale-up has been successfully carried out. However, these methods require complex equipment, usually consisting of multiple columns, along with sophisticated systems for controlling the inlet and outlet streams of the mobile phase. Systems enabling the movement of the stationary phase are also necessary in some cases [20]. Although TMB and SMB chromatography are continuous processes, they do not operate under steady-state conditions. In contrast, FFE generally operates continuously under steady-state conditions when carefully implemented. The apparatus consists of a single module, and control is required only for the electrolyte flow, applied electric current, and temperature [22]. Nevertheless, current FFE systems, which are typically designed as microfluidic or millifluidic devices, are not suitable for the production of larger product quantities. A potential solution could be a massive parallelization of FFE – the numbering-up approach [23,24]. Prior to this, a thorough understanding of the coupled transport and reaction phenomena occurring in FFE systems is necessary.

Challenges associated with the use of FFE include the parabolic flow profile, potential flow irregularities due to improper pressure and flow control, and the coupling with electrode compartments, different electrolytic conductivities of a sample and carrier electrolyte, release of the Joule heat [21,25] etc. Another limiting factor is the relatively low level of understanding of the chemical and multiphysical couplings of the separation process. The transport of all chemical components is influenced by the combined effects of the applied pressure and electric fields. The electric field directly affects the movement of all ions within the separation chamber and the adjacent electrode reservoirs. The migration of individual ions with different electrophoretic mobilities is not independent but constrained by the requirement of approximate local electroneutrality [26,27]. The present chemical substances may also undergo dissociation reactions and exist in multiple ionic forms depending on the local pH value. To date, mathematical models of FFE [28,29] or other orthogonally operating devices [12,30,31] have been developed only to a limited extent. Analyte trajectories can be approximately predicted based on the estimation of characteristic velocities associated with pressure driven convection and electromigration transport [12,28,30]. More advanced models account for the electrostatic interactions among ions present in the carrier electrolyte and sample, incorporating the local electroneutrality condition and the electric charge balance. Zheng et al. [29] applied such a model to a FFE device with a recycle loop to predict the spatial distribution of concentration and electric conductivity. Yoo et al. [31] used a similar model to investigate free flow isoelectric focusing for protein separation. However, the application of the full Poisson-Nernst-Planck-Navier-Stokes concept [32] remains highly challenging due to the a priori unknown distribution of free electric charge in the system.

We aimed to investigate in detail the behavior of separated enantiomers in an FFE device under varying carrier electrolyte concentrations and different applied electric currents. Our study includes experimental measurements using a lab-made FFE apparatus, as well as the derivation and numerical analysis of a mathematical model of FFE. The investigated system consisted of a mixture of mandelic acid (MA) enantiomers in the presence of a chiral selector based on β-cyclodextrin, whose ability to selectively bind one of the mandelic acid enantiomers was also examined using capillary electrophoresis. The core part of the work involves the comparison of experimental results and model predictions focused on the distribution of mandelic acid under various FFE regimes. The mathematical model is based on the application of momentum, mass, component, and electric charge balances, coupled with the local electroneutrality condition. Based on this comparison, it was possible to identify suitable conditions for effective enantiomer separation and to explain otherwise difficult-to-predict behavior of the separation system. Experimental verification of the enantioseparation capability of the fabricated device confirmed that continuous enantiomer separation is feasible.

2. Experimental

2.1. Materials and chemicals

In capillary electrophoresis experiments, we tested the following chiral selectors: 6-monodeoxy-6-monoamino-β-cyclodextrin hydrochloride (MMBCD) (CycloLab Ltd., Hungary), (2-hydroxy-3,*N*,*N*,*N*-trimethyl-amino)propyl-β-CD (APBCD) (CycloLab Ltd., Hungary, degree of substitution 3.2), (2-hydroxypropyl)-β-CD (HPBCD) (Sigma-Aldrich, Japan, degree of substitution 0.6), heptakis(6-Amino-6-Deoxy)-β-CD (ADBCD) (CycloLab Ltd., Hungary), β-CD (BCD) (Sigma-Aldrich, Japan), carboxymethyl-γ-CD (CMGCD) (AraChem, Netherland, degree of substitution 3.2), carboxymethyl-β-CD (CMBCD) (CycloLab Ltd., Hungary, degree of substitution 4.3).

The other used chemicals are: formic acid, ortho-phosphoric acid (50 %, Sigma-Aldrich, Czech Republic), acetic acid (99 % Sigma-Aldrich, Czech Republic), thiourea (99 % Sigma-Aldrich, Czech Republic), ultrapure water (Milli-Q grade, Millipore, France), 1 M sodium hydroxide (Tripur, Merck, Germany), hydrochloric acid (30 %, Suprapur, Merck, Germany), PBS buffer (Sigma-Aldrich, P38135), sodium dihydrogen phosphate dihydrate (Penta, 13472–35-0), sodium dibasic phosphate dihydrate (Fluka, 71645), racemic mandelic acid (Sigma-Aldrich, M2101) and an azo-tracer dye trypan blue (Sigma-Aldrich, T6146).

For the fabrication of the FFE device we used PMMA (polymethyl methacrylate) sheets, Tygon tubings with internal diameter of 1.22 mm, a 23-μm-thick cellulose membrane Membra-Cel MD34 (14-kDa-MWCO), 3D printing UV resin Flexible-X (Liqcreate), UV curable acrylate glue Acrifix 192 (Evonik) and low viscosity Acrifix 117 (Evonik).

2.2. Fabrication of FFE device

The FFE device shown in Fig. 1(a) and (b) was fabricated from several PMMA plates supplemented with various functional components. Electrolyte was continuously introduced through a series of inlets (A) located at one end of the separation chamber (B). The remaining inlet for the sample (C) was positioned centrally in the middle of channel, upstream of the electrolyte inlets. The liquid exited the

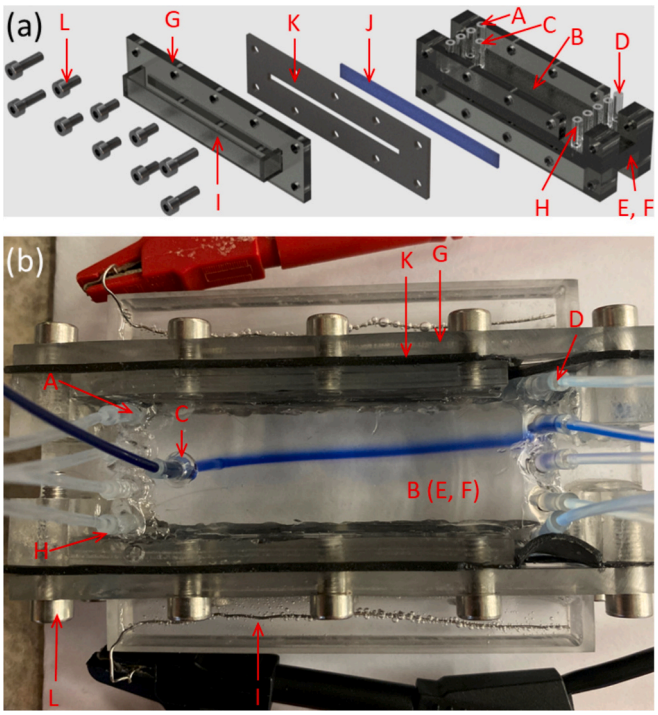

Fig. 1. Schema (a) and photo (b) of the FFE device: (A) the inlets of the carrier electrolyte, (B) the separation chamber. (C) The sample inlet. (D) The electrolyte outlets. (E) The top and bottom PMMA plates (walls) of the separation chamber. (F) The insert between the PMMA plates. (G) The PMMA blocks with holes. (H) Tygon tubing. (I) The electrode reservoirs. (J) The cellulose membranes. (K) The rubber gaskets. (L) Screws.

chamber through an array of outlets (D) situated on the opposite side of the device. The separation chamber (B) is characterized by its length L_R, width W_R, and depth d, and the separation distance of two adjacent outputs Δx, see Table 1. We fabricated two separation chambers with the depths of d_1 and d_2 for different types of experiments. The separation chamber consisted of the top and bottom 4-mm-thick PMMA plates (E), each 4-mm-thick, 100-mm-long and 30-mm-wide, separated by inserts (F) of the thickness d_1 or d_2. These plates were glued together with PMMA blocks (G) with holes for threads. A set of holes with the diameter of 1.20 mm diameter was drilled in the upper PMMA plate to provide the inlet and outlet ports for a carrier electrolyte and sample. We glued 10-mm-long Tygon tubing (H) to each opening to complete the inlet and outlet ports. To conductively separate the electrolytes in the separation chamber and in the electrode reservoirs (I), we used two 80-mm-long and 6-mm-wide cellulose membranes (J). Each electrode reservoir with internal dimensions of 75 mm × 9 mm × 9 mm was milled into a 10-mm-thick PMMA block. The FFE device was sealed using 1-mm-thick 3D-printed rubber gaskets (K) placed between the cellulose membrane (J) and the electrode reservoir (K). To prevent leakage fluid from the separation chamber, the device was tightly assembled by M4 screws (L).

We have developed a self-regulating liquid-level system to ensure uniform electrolyte flow through the separation chamber (not shown in Fig. 1). The system is based on five reservoirs, each connected to an outlet and open to the atmosphere, allowing for automatic equalization of the electrolyte levels due to the hydrostatic pressure. Without this self-regulating system, the liquid would preferentially exit through the outlet with the lowest hydrodynamic resistance causing an uneven flow distribution across the separation chamber.

Table 1
The main geometrical characteristics of the separation chamber.

Parameter	Value	Description
L_R	70 mm	Length of the separation chamber
W_R	30 mm	Width of the separation chamber
d_1	1 mm	Depth of the separation chamber
d_2	250 μm	Depth of the separation chamber
Δx	6 mm	Separation distance of two adjacent outputs

2.3. Capillary electrophoresis

We used the capillary electrophoresis (CE) method to identify a proper chiral selector and separation conditions for the MA enantiomers. CE was performed with an Agilent CE instrument 7100 (Agilent 3D HPCE, Waldbronn, Germany) equipped with a UV–Vis diode-array detector. A bare fused-silica capillary of 375 μm/75 μm od/id and 58.5 cm/50 cm total/effective length was purchased from Polymicro Technologies (Phoenix, AZ, USA).

A new fused-silica capillary was first rinsed with 1 M NaOH for 30 min, then with water for 30 min. Between runs, the capillary was rinsed first with 100 mM NaOH for 2 min, then with water for 2 min, and finally with the running buffer again for 2 min under 99.4 kPa. Analytes were hydrodynamically injected into the capillary at a pressure of 5 kPa for 5 s. Separations were performed at 20 kV (anode at the injection capillary end) with a voltage ramp time of 12 s. Detection using flow cell was carried out at 207 nm with the bandwidth of 4 nm. The capillary was thermostated at 25 °C. 50 mM buffers under a chosen pH was used as a background electrolyte (BGE).

The calculation of the apparent stability constants for MA-MMBCD complex is based on determining the migration times and effective mobilities at various concentrations of the chiral selector. MA enantiomers were separated using different concentrations of MMBCD. 2 mM thiourea was used as a marker for electroosmotic flow in these experiments. The separations were conducted at concentrations of MMBCD ranging from 0 mM to 16 mM. The observed migration times were used to calculate the apparent stability constants as described in [33].

2.4. Separation experiments

A carrier electrolyte was introduced through four inlets, while the sample solution was delivered via a dedicated sample inlet, as illustrated in Fig. 1. In the first set of experiments, we examined the capability of the FFE device to direct MA to a selected outlet under varying operational conditions, specifically different applied electric currents and carrier buffer concentrations. For this purpose, racemic MA dissolved in the carrier electrolyte was introduced through the sample inlet. The flow rate of the carrier electrolyte $\dot{V}_E$ was set to 200 μL min^{-1} per inlet, while the sample flow rate $\dot{V}_S$ was set to 20 μL min^{-1}. The depth of the separation chamber was $d_1 = 1$ mm in this set of experiments.

Enantioseparation experiments in the presence of a chiral selector were conducted using an FFE device with a reduced separation chamber depth of $d_2 = 250$ μm. This modification allowed operation under conditions of lower Joule heat generation and decreased chiral selector consumption. The flow rates of the carrier electrolyte $\dot{V}_E$ and the sample $\dot{V}_S$ were adjusted to 100 μL min^{-1} and 10 μL min^{-1}, respectively. The sample consisted of a solution containing both MA and MMBCD as the chiral selector, each at a concentration of 10 mM prepared in the carrier electrolyte. The carrier electrolyte was introduced through the four inlets without any chiral selector. Two different carrier electrolytes were used, 0.1 × PBS buffer and Sorensen buffer, to study the influence of pH on the separation performance of the FFE device. The concentration of the Sorensen buffer was adjusted so that its electrolytic conductivity matched that of 0.1 × PBS, i.e., approximately 1.3 mS cm^{-1}.

We found that Joule heating in the FFE device adversely affected the stability of the MA-MMBCD complex due to the disruption of non-covalent bonds. Thermodynamic studies of BCD complexes with MA and other aromatic enantiomers have shown negative values of both Gibbs free energy and enthalpy, indicating that the binding is

spontaneous and exothermic [34]. Consequently, according to the van't Hoff relationship, the stability association constants decrease with increasing temperature. To address this issue, the FFE device was placed on an aluminium block cooled from below by a STONECOLD Peltier cell (TEM Electronic Components, 40 mm × 40 mm). The Peltier cell was powered by an external source under the following conditions: current 1.5 A – 1.6 A and voltage 3.0 V – 3.5 V. The temperature at the interface between the aluminium block and the bottom plate of the FFE device was monitored and maintained at 15 °C, while the temperature at the top of the device did not exceed 25 °C during the separation experiments.

2.5. Chemical analysis

The total concentration of racemic MA in samples taken from the FFE device outputs was determined using a Tecan Infinite M200 spectrophotometer. Measurements were conducted with a quartz microplate (730–009-44, Hellma Analytics), utilizing 200 µL of each sample. Absorbance was recorded at 210 nm.

The concentration of MA enantiomers was determined by an Agilent 1260 HPLC system with a UV–Vis detector at a wavelength of 200 nm [35]. Enantiomer separation was achieved using a Nucleosil Chiral-1 column from Macherey-Nagel at a temperature of 50 °C. A 0.5 mM aqueous solution of copper (II) sulphate was introduced into the column as a mobile phase at a flow rate of 1 mL min^{-1}.

3. Mathematical model

Aqueous PBS electrolyte is a complex mixture containing sodium, chloride, potassium, hydrogen phosphate, dihydrogen phosphate, hydroxyl and hydrogen ions coupled by dissociation equilibria and the local electroneutrality. Moreover, both mandelic acid enantiomers can appear in protonated and deprotonated forms. For the purpose of the mathematical model, we introduce these simplifications: (i) pH value is constant and equal to 7.4, (ii) the PBS electrolyte is represented only by sodium cation (C) and chloride anion (A), (iii) mandelic acid enantiomers are present only as anions ($pK_a = 3.41$). These simplifications are approximately satisfied when the mandelic acid concentration is comparable or lower than the PBS concentration.

The selected chiral selector BCD binds both enantiomers; however, with a higher stability constant to RMA (presented in Section 4.3). This means that both enantiomers are present in the sample in both free and bound forms. However, in the mathematical model, we assume ideal behavior, i.e., RMA is completely bound to BCD and is referred to as DMA in the following text. Conversely, SMA does not bind to BCD at all and is referred to as FMA.

3.1. Steady state governing equations

Because we assume the local electroneutrality in the separation chamber, we can decouple governing equations for the momentum transfer and the other equations describing the distributions of electric potential and ion concentrations. The velocity ($\boldsymbol{v}$) and pressure (p) fields in an aqueous electrolyte are described by the Navier-Stokes and continuity equations

$$\rho \boldsymbol{v} \bullet \nabla \boldsymbol{v} = -\nabla p + \mu \nabla^2 \boldsymbol{v}, \qquad \nabla \bullet \boldsymbol{v} = 0, \tag{1}$$

where the symbols ρ and μ are the electrolyte density and viscosity, respectively. The gravity term is not considered due to horizontal orientation of the model domain (Fig. 2). As boundary conditions, we set particular flow rates with corresponding laminar velocity profiles at the sample and electrolyte inlets, a reference zero pressure at all outlets, and zero velocity vector on the other boundaries.

The steady-state concentration fields of ions (c_i) are given by solving the molar balances

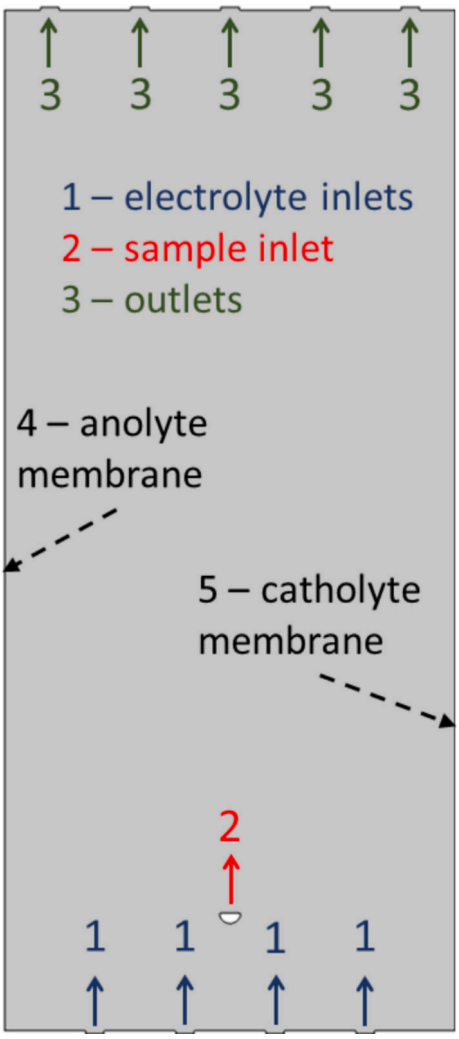

Fig. 2. Geometry of the model domain with labeled boundaries. Impermeable walls of the separation chamber among the inlets and outlets are unlabeled. Dimensions of the domain are identical to the experimental separation chamber.

$$\nabla \bullet (\boldsymbol{v} c_i - D_i \nabla c_i - z_i D_i F c_i \nabla \phi / (R_T T)) = 0, i = \mathrm{FMA}, \mathrm{DMA}, \mathrm{A}, \mathrm{C} \tag{2}$$

The three terms in Eq. (2) represent the convection, diffusion and electromigration fluxes of the ions in diluted electrolytes [36], respectively. The symbols D_i, z_i, F, R_T, T, and ϕ are the ion diffusivity, the ion charge number, the Faraday constant, the molar gas constant, temperature, and electric potential. A linear combination of the molar balances Eq. (2) results in the local balance of electric charge that in a steady state reads

$$\nabla \bullet F \sum_i z_i (\boldsymbol{v} c_i - D_i \nabla c_i - z_i D_i F c_i \nabla \phi / (R_T T)) = 0, i = \mathrm{FMA}, \mathrm{DMA}, \mathrm{A}, \mathrm{C} \tag{3}$$

We do not assume the existence of free electric charge as it happens at interfaces with bound electric charge [32]. Instead of one molar balance, Eq. (2), for one ion, we use the local electroneutrality condition [26].

$$F \sum_i z_i c_i = 0, i = \mathrm{FMA}, \mathrm{DMA}, \mathrm{A}, \mathrm{C} \tag{4}$$

Eq. (2) for all ions except one, Eq. (3), and Eq. (4) form a set of linearly independent equations that we numerically solve to determine the fields of ion concentrations and electric potential.

We consider the reference zero electric potential on the catholyte membrane. A particular electric potential is set to the anolyte membrane. All other boundaries are treated as electric insulators. At all electrolyte inlets, zero concentrations of FMA and DMA and a specific non-zero concentration of A are considered. The same concentration of A is also considered at the sample inlet, along with the chosen concentrations of FMA and DMA. The concentration of C is always calculated based on the condition of electroneutrality, Eq. (4). At all outlets, as well as on the anolyte and catholyte membranes, the continuity of convective and electromigration fluxes of all ions is considered, which is equivalent to the existence of a zero normal derivative of the concentrations of all ions at these boundaries. Zero fluxes of all ions are set to all impermeable walls.

3.2. Numerical analysis

We used Comsol Multiphysics software equipped with a CFD module to solve the model Eqs. (1)–(4). We first calculated steady state fields of velocity and pressure solving Eq. (1) in the CFD module. We then fixed these fields and solved Eqs. (2)–(4) to obtain steady state distributions of ion concentrations and electric potential for selected values of electric potential on the anolyte membrane. We formulated Eqs. (2)–(4) using their general forms [37].

Sharp edges at the inlets and outlets of the computational domain were rounded with an arc with a radius of 0.1 mm. We discretized the domain into a mesh of approximately 311 thousand triangular elements with a maximum edge length of 0.15 mm. The maximum edge length of boundary elements at the inlets and outlets was set to 0.1 mm. The model equations were solved using MUMPS stationary solver [38,39] with relative tolerance 0.001.

Parameter values used in numerical simulations are summarized in Table 2. The diffusivity of BCD-SMA complex (DMA) was assumed to be equal to diffusivity of BCD-ibuprofen complex in water [40].

4. Results and discussion

4.1. Flow distribution in FFE device

For correct operation of FFE in a steady state, it is necessary to provide symmetric and stable laminar flow of electrolyte [25]. In our system, the inlet flow rates are precisely controlled by the syringe pumps. Even distribution of flow rates at the outputs is guaranteed by the hydrostatic pressure control at the outputs. The steady state trajectory of a tracer trypan blue (TB) in FFE without any applied electric field is shown in Fig. 3a. The trajectory was stable and straight as expected and anions of MB exit through the central output.

Another problem related to FFE devices is focusing of an analyte to a particular output. A concentration trajectory should be as narrow as possible, not too affected by the Taylor dispersion [42]. The width of the trajectory can be influenced by the flow rates of the sample $\dot{V}_S$ and the electrolyte $\dot{V}_E$ at each inlet. We found that a concentration trajectory of appropriate width is achieved with the total electrolyte flow rate ($4\dot{V}_E$) approximately 40 times greater than that of the sample ($\dot{V}_S$), Fig. 3a. A higher ratio leads to significant sample dilution, while a lower ratio results in a too wide trajectory. Theoretical flow and velocity distributions for these conditions are shown in Fig. 3b. One can see that all streamlines emerging from the sample inlet end at the middle FFE outlet.

The ability of the designed device to address the trajectory toward a non-central outlet using an electric field is demonstrated in Fig. 3(c). At pH 7.4, TB ions carry an electric charge of minus 4 and their trajectories are deflected toward the anode in the presence of an electric field. At the selected electric current, the TB ions exit through the second outlet from the left.

Table 2
Model parameters.

Parameter	Value	Description
D_A	2.0×10^{-9} m^{2}s^{-1}	Diffusivity of chloride anions [36]
D_C	1.33×10^{-9} m^{2}s^{-1}	Diffusivity of sodium cations [36]
D_{FMA}	8.6×10^{-10} m^{2}s^{-1}	diffusivity of FMA [41]
D_{DMA}	3.3×10^{-10} m^{2}s^{-1}	diffusivity of DMA [40]
F	96,485 C mol^{-1}	The Faraday constant
R_T	8.314 J mol^{-1} K^{-1}	Molar gas constant
T	298 K	Temperature
z_A	-1	Charge number of chloride anions
z_C	1	Charge number of sodium cations
z_{FMA}	-1	Charge number of FMA
z_{DMA}	-1	Charge number of DMA
μ	0.891 mPa s	Viscosity
ρ	997 kg m^{-3}	Density

4.2. FFE of racemic mixture

A proper setting both electrolyte flow rate and applied electric current represents another challenge related to FFE devices. A good estimate of electric current that is necessary for addressing a concentration trajectory to a particular outlet of any FFE device results from the consideration that the residence time of sample t_R must be approximately equal to the electromigration time of an enantiomer in the orthogonal direction t_E

$$t_R = \frac{L_R}{(\dot{V}_S + 4\dot{V}_E)/(W_R d)}, t_E = \frac{\Delta x}{u_E} \tag{5}$$

where the symbols L_R, d, W_R, Δx are the geometrical characteristics of the FFE separator, see Table 1. The electromigration velocity of an enantiomer u_E reads

$$u_E = \frac{z_{MA} D_{MA} F i_c}{R_T T \sigma} \tag{6}$$

with the electric current density and electrolytic conductivity calculated according to

$$i_c = \frac{I}{L_R d}, \sigma = F^2 \Big/ (R_T T) \sum_i z_i^2 D_i c_i \tag{7}$$

where the symbols I, d, and L_R are the applied electric current, the thickness and length of separation chamber ($L_R d$ is the cross-sectional area perpendicular to the direction of electric current flow), respectively. In the sum for electrolytic conductivity, the charge numbers, diffusivities, and concentrations of all ions present in the electrolyte must be included [36].

Combining Eqs. (5)–(7) we obtain an explicit expression for electric current that ensures the deflection of the concentration trajectory of the enantiomer to the desired output

$$I = \frac{(\dot{V}_S + 4\dot{V}_E)\Delta x F \sum_i z_i^2 D_i c_i}{z_{MA} D_{MA} W_R} \tag{8}$$

To study the effects of the electric current on the distribution of MA at the FFE device outputs, we define a quantity f_n as the fraction of MA leaving n-th output relative to the total input of MA. For the sum of these fractions, we can write a simple inequality

$$0 \le \sum_{n=1}^{5} f_n \le 1 \tag{9}$$

If the sum is less than 1 then certain fraction of the introduced MA escapes through the anolyte or catholyte membrane into the electrode reservoirs.

Using Eq. (8), it is possible to estimate the predominant output of the FFE device for MA at a given supporting electrolyte concentration and a specified electric current value. For example, 19.1 mA is estimated to efficiently deflect the concentration trajectory of MA in 0.1 × PBS to the

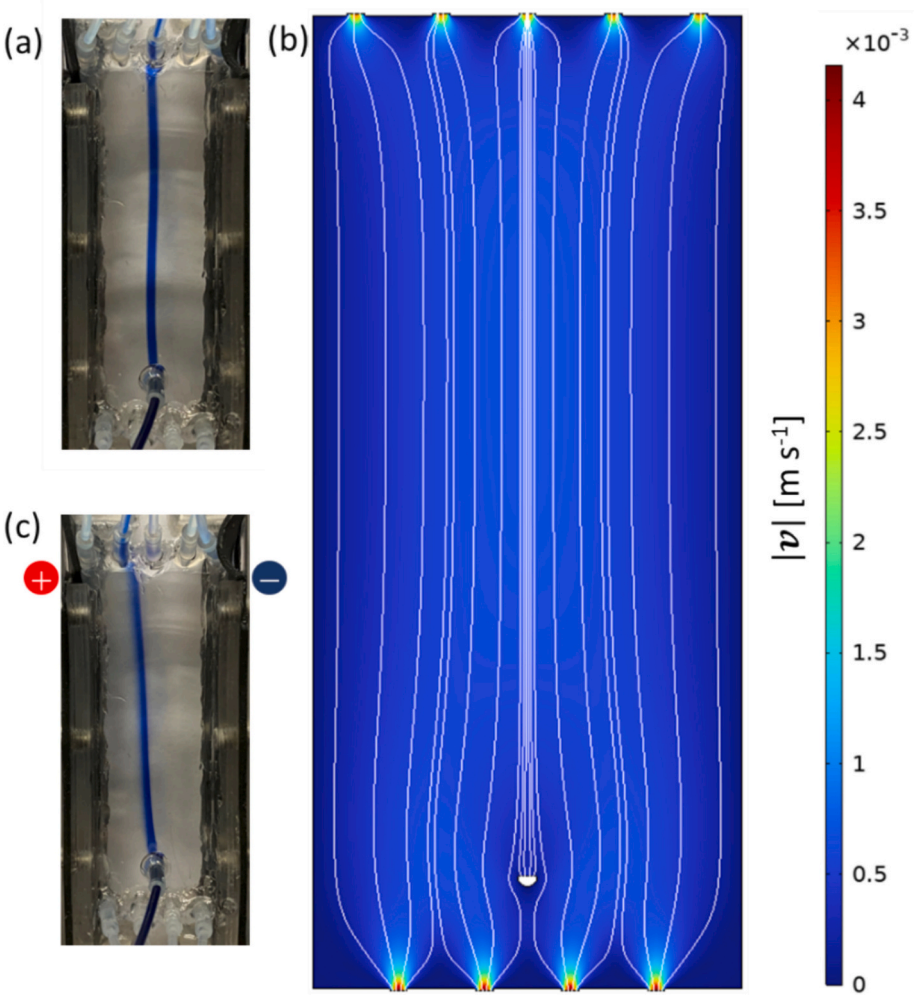

Fig. 3. (a) Steady state trajectory of TB in FFE device, $I = 0$ A. (b) Streamlines and velocity magnitude in FFE device predicted by the mathematical model, $d = 1$ mm, $\dot{V}_S = 20$ μL min^{-1}, $\dot{V}_E = 200$ μL min^{-1}. (c) Steady state trajectory of TB in FFE device $I = 7.5$ mA., Sorensen buffer pH = 7.4.

first output from the center. This estimated is in good agreement with our experimental observations and the results of the mathematical model as it can be seen in Fig. 4(b).

In Figs. 4 (a)–(c), the experimentally determined distribution of MA in the individual outputs of the FFE device at various applied electric current values and supporting electrolyte concentrations is represented by black lines and symbols. The predictions of the mathematical model described in Section 3.1 are shown by red lines.

For the selected electric currents ranging from 40 mA to 80 mA at the highest supporting electrolyte concentration of 1 × PBS, a qualitative and quantitative agreement was achieved, as shown in Fig. 4(a). We therefore assume that the concentration trajectories of MA calculated using the mathematical model, Fig. 4(d), reflect the real behavior of the FFE device. The concentration trajectories are narrow, exhibiting only minor lateral dispersion, and trajectory broadening is noticeable only at the device outlets, which is caused by the distortion of the velocity field, see Fig. 3(b). In agreement with the approximate relation given by Eq. (8), high electric current values are required to achieve significant deflection of the trajectory from the straight flow direction. At 80 mA, MA leaves through outlets 2 and 3 (the third outlet being central), in an approximately 1:1 ratio. However, the necessity of applying high electric currents brings disadvantages such as intense electrode reactions including gas formation and temperature elevation due to Joule heating.

Good agreement between the results of the mathematical model and the experimental data was also achieved for lower concentrations of the supporting electrolyte, 0.1 × PBS and 0.01 × PBS, as shown in Figs. 4(b) and 4(c). However, to experimentally achieve similar MA distributions at the device outlets, higher electric currents had to be applied than those predicted by the mathematical model. For example, to address the majority of MA through the outlet 2 at a supporting electrolyte concentration of 0.1 × PBS, an electric current of 30 mA was required experimentally, while the model predicts a sufficient value of 20 mA. Even larger relative differences between the predicted and experimentally applied currents are observed for a supporting electrolyte concentration of 0.01 × PBS.

This discrepancy is attributed to the use of a highly concentrated buffer (10 × PBS) in the electrode reservoirs during the experiment, which was intended to concentrate the majority of the electric potential drop within the separation chamber. Consequently, ion concentration in the separation chamber increased due to electromigration and diffusive transport from the electrode reservoirs. Nevertheless, the mathematical model is still able to qualitatively predict the behavior of the experimental device.

A decreasing concentration of the supporting electrolyte leads to a reduction of the electric current required to deflect the concentration trajectory toward outlet 2 or 1. As a result, electrode reactions as well as potential heating of the FFE system due to Joule heating are suppressed. However, as shown in Figs. 4(e) and (f), a lower supporting electrolyte concentration leads to significant lateral dispersion of MA. In particular, at a supporting electrolyte concentration of 0.01 × PBS, it is no longer possible to focus the MA trajectory into a single outlet. In an extreme case, MA even escapes into the electrode reservoir. Operating the FFE

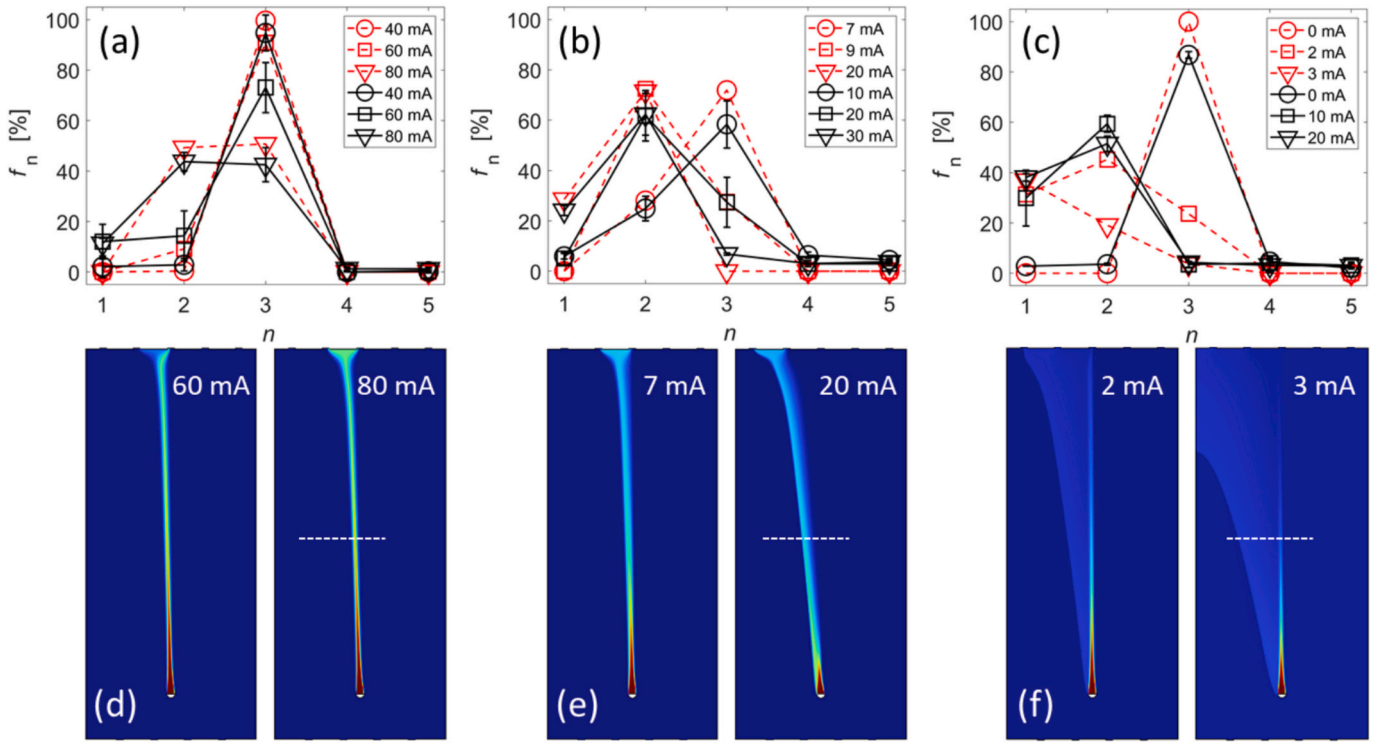

Fig. 4. Effects of the carrier buffer concentration (a) 1 × PBS. (b) 0.1 × PBS. (c) 0.01 × PBS and applied electric current on distribution of MA at the outlets of FFE device, experimental results (black), theoretical predictions (red). Steady state concentration field of MA in FFE under different electric currents and buffer concentrations (d) 1 × PBS, (e) 0.1 × PBS, (f) 0.01 × PBS. Profiles of model variables were further analyzed along the cross-sections marked by white dashed lines in panels (d)–(f). The other parameters are: $d_1 = 1$ mm, $\dot{V}_S = 20$ μL min^{-1}, $\dot{V}_E = 200$ μL min^{-1}, $c_{MA}^{in} = 10$ mM. (For interpretation of the references to color in this figure legend, the reader is referred to the web version of this article.)

device under such conditions therefore offers only limited potential for the effective separation of chemicals with different electrophoretic mobilities. The origin of the lateral dispersion is discussed below.

In Fig. 5, we plotted distributions of selected model variables in spatial cuts through the two-dimensional domain as depicted by dashed white lines in Fig. 4. In addition to the concentrations of individual ionic species and the electric potential, two auxiliary variables were plotted in the graphs: the ionic strength, s, and the x-component of the electric field, E_x, which are defined by the following relationships

$$s = \sum_i z_i^2 c_i \Big/ 2, E_x = -\partial\phi \Big/ \partial x \tag{10}$$

By comparing Figs. 4 and 5, it can be observed that local changes in the total ionic strength of the electrolyte occur in the region where the MA anion is present. In Fig. 5, a local decrease of the ionic strength, referred to as an ion-depleted zone, can always be seen, followed by a gradual increase in ionic strength, known as an ion-enriched zone [32,43–46]. These depleted and enriched zones are indicated by color lines in Fig. 5. The depleted zone is always located closer to the anode, while the enriched zone lies nearer to the cathode. The overall width of the region exhibiting local changes in ionic strength increases with decreasing concentration of the supporting electrolyte.

Fig. 5 further shows that the total ionic strength is always equal to the concentration of the cation and simultaneously to the sum of the concentrations of the anion of the supporting electrolyte and the MA anion, as follows from Eqs. (4) and (10). In the ion-depleted and ion-enriched zones, significant changes in the electric field occur. For the highest concentration of the supporting electrolyte (1 × PBS), the electric potential profile is nearly linear, and the electric field is locally intensified or weakened by only a few percent. In contrast, for the lowest electrolyte concentration (0.01 × PBS), distinct changes appear in the otherwise monotonic electric potential distribution, leading to electric field fluctuations in the order of several kV m^{-1}. In the depleted zone, the electric field is always the strongest, while in the enriched zone it is the weakest, ensuring continuity of ion fluxes and electric current between the respective zones.

The observed phenomenon is very similar to the formation of ion-depleted and ion-enriched regions near cation-exchange membranes [47]. These membranes contain fixed negative charges, which hinder the passage of anions while allowing cations to pass freely through the membrane. As a result, anions migrating in the direction from the cathode toward the membrane accumulate in front of it, forming an enriched electrolyte layer [32,48]. The cation concentration also increases in the enriched region, as required by the condition of local electroneutrality, see Eq. (4). On the side of the cation-exchange membrane facing the anode, a depleted zone is formed [49]. This occurs because anions are both repelled by the fixed negative charge within the membrane and migrate toward the anode due to the applied electric field. The cation concentration also decreases in the depleted region in order to maintain the electroneutrality condition.

The principle underlying the formation of ion-depleted and ion-enriched regions in the studied FFE device is analogous to that observed in systems with cation-exchange membranes, with the difference that instead of a fixed negative charge, MA anions are present. For a hypothetical analyte with diffusivity approaching zero, the behavior of the FFE system would be identical to that of a system incorporating a cation-exchange membrane. Here, MA anions exhibit diffusivity approximately one order of magnitude lower than that of the other ions in the system (Table 2). The region containing MA ions behaves similarly to a cation-exchange membrane by partially hindering the transport of anions with higher mobility. This effect becomes more pronounced as the concentration of MA ions increases relative to the concentration of the anions in the supporting electrolyte. The formation and expansion of the depleted zone leads to lateral dispersion, as illustrated in Fig. 4,

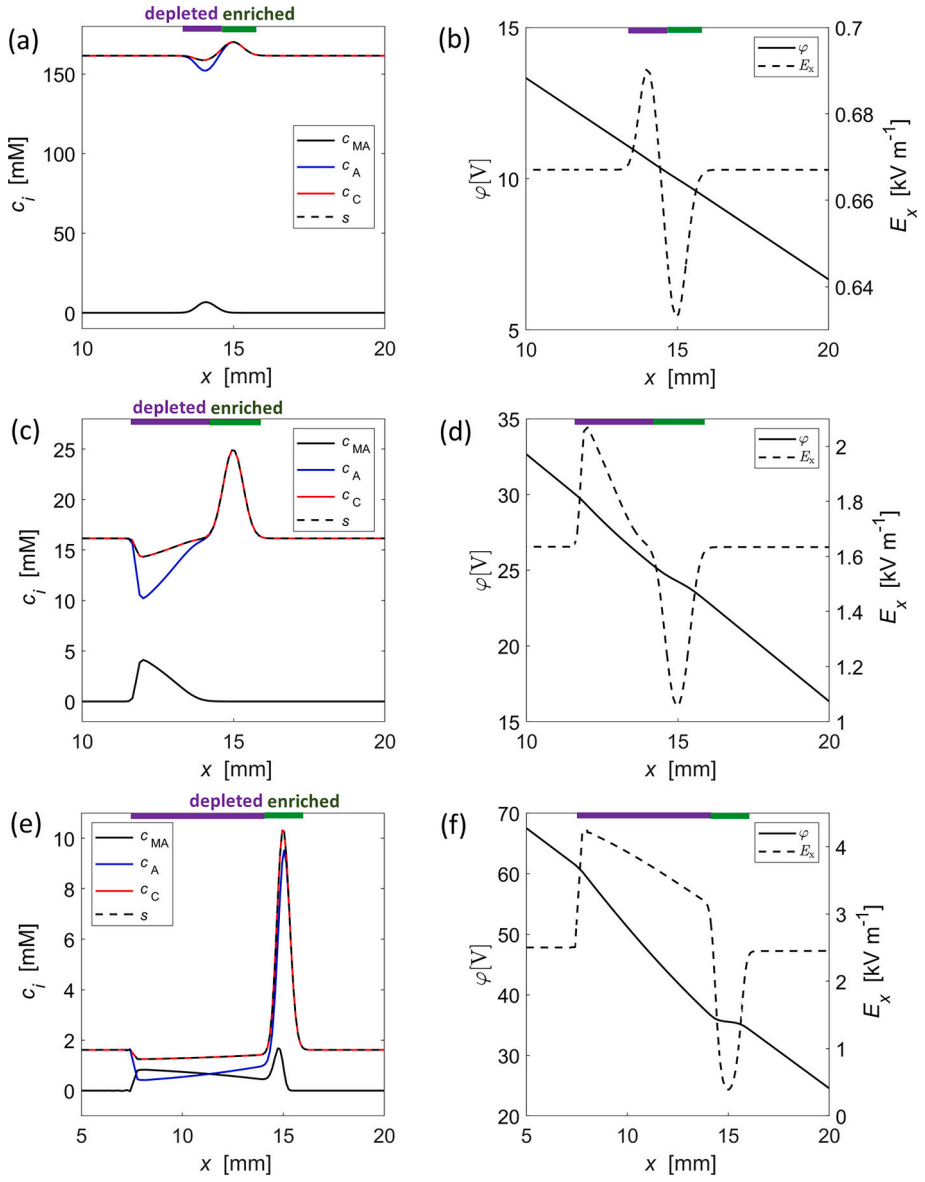

Fig. 5. Spatial profiles of the ion concentrations and ionic strength (a, c, e) and spatial profiles of the electric potential and the *x*-component of electric field, E_x (b, d, f) along the cuts in Fig. 4 highlighted by the white dashed lines. (a, b) 1 × PBS, $I = 80$ mA, (c, d) 0.1 × PBS, $I = 20$ mA, (e, f) 0.01 × PBS, $I = 3$ mA. The spatial extent of the ion depleted and ion enriched zones observed along the cuts are indicated at top of plot boxes by color lines.

which makes difficult the effective separation of MA ions from the mixture.

Our results indicate that the minimum concentration of the supporting electrolyte should be at least equal to the concentration of the separated analyte. This condition is approximately satisfied with the 0.1 × PBS buffer, as shown in Figs. 4 and 5. While higher concentrations of the supporting electrolyte result in intense electrode reactions, lower concentrations lead to undesirable dispersion. For this reason, experiments focused on the separation of MA enantiomers were conducted in 0.1 × PBS buffer.

Our mathematical model shows good agreement with the experimental results obtained. In addition, it allows prediction of the effects of ion enriched and ion depleted zones on the separation performance of FFE devices and provides a clear demonstration of the fundamental mechanism responsible for the formation of these zones. Nevertheless, in many cases the model requires further extensions in order to be more generally applicable to chiral separations in the orthogonal FFT system.

Such extensions include, for example, incorporation of an energy balance, since Joule heating, electrolyte flow, and the material properties of the FFT device influence the temperature distribution within the system. It may also be advantageous to include material balances for all ionic species present in the electrolyte, as ions with different mobilities mutually interact through electrostatic forces [36], leading to the development of enriched and depleted zones. When a buffer is used as the carrier electrolyte, it is appropriate to include balances for all dissociated and undissociated components, including hydrogen and hydroxyl ions, either under the assumption of instantaneous dissociation equilibrium [26] or by accounting for finite dissociation kinetics [50]. Furthermore, it is advisable to incorporate the experimentally determined stability (association) constant for a specific equilibrium complex of the separated enantiomer with a chosen chiral selector [51]. In that case, the model must also include balances for the chiral selector itself, its two complexes with the enantiomers, and the two free enantiomers.

4.3. *Screening of chiral selectors*

Based on our previous experience [52], initial analyses were

performed at a concentration of 10 mM β-cyclodextrins in a 50 mM phosphate buffer at pH of either 2.5 or 7.0 (adjusted to appropriate pH with 1 M NaOH or 35 % HCl). The resolution of enantioseparations R_S reads

$$R_S = \frac{t_{m2} - t_{m1}}{0.85(W_1 + W_2)} \quad (11)$$

where t_{m1} and t_{m2} are migration times for the first and second migration peak and W_1 and W_2 are peak widths at their half heights. The best enantioseparation was achieved by using MMBCD with a permanent positive electric charge that supports the electrostatic interaction with dissociated MA enantiomers. Additionally, we achieved a resolution less than one for MA enantiomers using ADBCD. The other tested cyclodextrins (APBCD, HPBCD, BCD, CMBCD, CMGCD) were unable to chirally separate MA enantiomers under the chosen conditions.

We investigated the effect of BGE pH value on the separation performance in the next step. Racemic MA at a concentration of 1 mM was separated across a pH range of 2.5 to 7.0. The BGE always consisted of 50 mM buffer and 10 mM MMBCD. Different buffers were used to achieve selected pH values: (i) formate buffer for pH 3.5, (ii) acetate buffer for pH 4.75, and (iii) phosphate buffers for pH 2.5 and 5.9–7.0. The best resolution was achieved with a 50 mM phosphate buffer at pH 6.3 as it is summarized in Table 3. In all these experiments, the RMA and SMA were used in the ratio of 3:7 to identify the first migrating enantiomer. We found that the first migrated enantiomer is RMA under pH = 6.3 (Fig. 6). The calculated apparent stability constants at pH 6.3 for the complexes of RMA and SMA with MMBCD are 49 ± 4 M^{-1} and 40 ± 4 M^{-1}, respectively. Although the difference is modest, it is sufficient to achieve a resolution significantly greater than one in capillary electrophoresis.

4.4. Enantiomer separation in FFE device

To verify the enantioseparation capabilities, we fabricated a modified FFE device. The depth of the separation chamber was reduced to 250 μm, and the flow rates of both the carrier electrolyte and the sample were decreased, as describe in Section 2.4. These modifications led to a reduced consumption of the chiral selector and decreased the amount of Joule heating generated by the electric current, which was set to 8.5 mA in all enantioseparation experiments. Instead of the 0.1 × PBS buffer, the Sorensen buffer of the same ionic strength was used as the carrier electrolyte. The pH of the carrier electrolyte was adjusted to 6.0, 6.5, and 7.0 by changing the buffer composition, targeting values near pH 6.3, at which the best resolution was achieved in CE experiments (see Table 3).

Prior the separation experiments, the FFT device was evaluated by visualizing TB trajectories. This test verified that no significant deformation of the trajectories or lateral diffusion occurred and that the applied electric field was able to direct the dye into the designated channel. Only FFT devices that passed this verification were subsequently employed in the experiments.

An electric current of 8.5 mA at the given flow rate through the separation chamber enabled the sample to be split into two adjacent outlets, labeled 2 and 3 in Fig. 7. Figs. 7(a)–(c) show the concentrations of SMA, RMA, and the total MA concentration at the device outlets, respectively, after reaching steady state conditions. Under the selected

Table 3
Resolution of MA enantiomers. U is the applied voltage. Positive voltage corresponds to the cathode at the detector end, while negative voltage indicates the anode at the detector end.

pH	2.50	3.50	4.75	5.90	6.30	6.45	7.00
U [kV]	−20	−20	−20	−20	+20	+20	+20
R_S	2.3	2.2	3.6	3.2	5.7	5.5	4.2
First migrating enantiomer	SMA	SMA	SMA	SMA	RMA	RMA	RMA

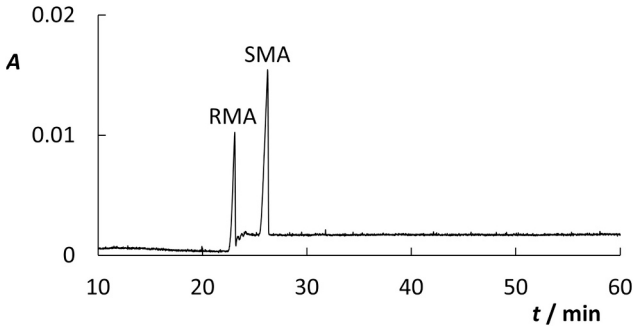

Fig. 6. Electropherogram of analyzed mixtures of MA enantiomers (RMA:SMA = 3:7); dependences of absorbance at 207 nm on electromigration time; 50 mM phosphate buffer with 10 mM MMBCD; pH = 6.3; U = 20 kV; detection at 207 nm; fused-silica capillary with the total/effective lengths of 58.5 cm / 50.0 cm, capillary i.d. 75 μm; temperature 25 °C.

electric current, approximately twice the amount of mandelic acid exits through port 2 compared to port 3. No presence of MA enantiomers was detected at port 4 or the outermost outlet ports 1 and 5. The concentration profiles of both enantiomers are qualitatively similar.

To assess the separation efficiency of the FFE device, we define the enantiomeric ratio

$$r_{S/R} = c_{SMA}/c_{RMA}, \quad (12)$$

where c_{SMA} and c_{RMA} denote the concentrations of the MA enantiomers at the FFE device outlets. The results in Fig. 7(d) indicate that outlet 2, located closer to the anode (Fig. 3(c)), contains a mixture enriched with the SMA enantiomer. This is because SMA has a lower affinity toward the chiral selector MMBCD and therefore exhibits higher mobility in the electric field. Conversely, the RMA enantiomer more readily forms a complex with the positively charged chiral selector. Due to the zero net charge and high molecular weight of this complex, the electrophoretic mobility of RMA effectively decreases, causing it to remain preferentially in the central outlet 3.

The enantiomeric ratio does not deviate significantly from unity in either of these outlets, which is attributed to the small difference in the stability constants between the chiral selector and the MA enantiomers. High enantiomeric excesses were not achieved even in some previous studies focused on separation using FFE [7,8,15]. High enantiomeric excess in certain output fractions was primarily obtained using the experimental Octopus system [14,17]. Our results demonstrate that the stability constants between MMBCD and the MA enantiomers plays a crucial role in achieving effective separation, underscoring the importance of selecting an appropriate chiral selector.

Fig. 7(d) shows that the error bars for measurements at outlets 2 and 3 do not overlap for any of the tested pH values. The ability of the device to partially separate MA enantiomers is therefore statistically significant: the enantiomeric ratio at outlet 2 is always greater than 1.0, and at outlet 3 always less than 1.0. The deviation of $r_{S/R}$ from 1.0 at outlet 2 is smaller in the absolute value than the deviation at outlet 3, because approximately twice the amount of MA exits through outlet 2 compared to outlet 3.

To achieve higher $r_{S/R}$ values, a more selective chiral selector or a different affinity pair would need to be used. For example, a quinine-based chiral selector for the protected amino acid dinitrobenzoyl-tert-leucine achieves an enantioseparation factor (i.e., the ratio of stability constants of the two enantiomers) as high as 88.5 [53]. Another example involves cyclodextrin-based chiral selectors used for the separation of tapentadol stereoisomers, where this ratio reaches values around 10 [54]. In our study, this ratio is only 1.225.

Our study confirms that the use of a highly selective chiral selector is essential for achieving effective separation in an FFE device. It also provides important insights into how the separation conditions should

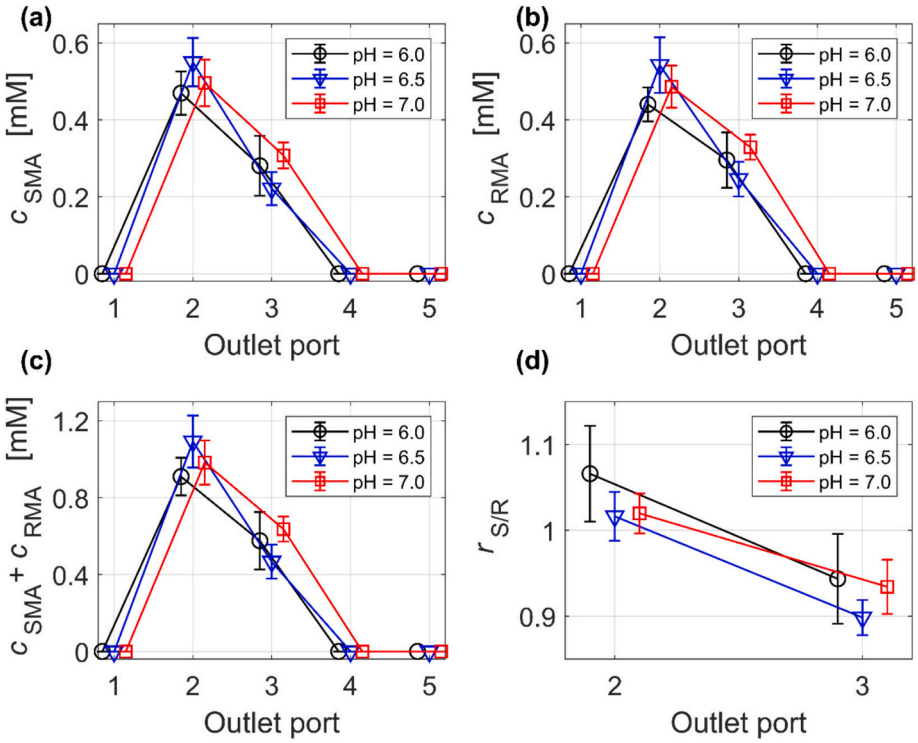

Fig. 7. Distributions of the concentrations of MA enantiomers at the outlets of FFE device: (a) SMA concentration. (b) RMA concentration. (c) The total concentration of MA. (d) Enantiomeric ratio. The distributions are slightly offset from each other to clearly display the measurement means and error bars. Carrier electrolyte: Sorensen buffer with selected pH values, $I = 8.5$ mA. The other parameters are: $d_2 = 250$ μm, $\dot{V}_S = 10$ μL min^{-1}, $\dot{V}_E = 100$ μL min^{-1}, $c^{in}_{MA} = 10$ mM.

be optimized, particularly with regard to the carrier electrolyte concentration.

5. Conclusions

This study demonstrates that lateral FFE, when combined with a carefully selected chiral selector, can serve as a viable method for continuous enantiomer separation. We revealed that the transport behavior of enantiomers in FFE is strongly influenced by the concentration of the carrier electrolyte and the nature of electrostatic interactions within the system.

A key outcome of this work is the identification of ion-depleted and ion-enriched zones around the enantiomeric concentration trajectories, which are analogous to phenomena observed near ion-exchange membranes. These zones significantly affect the lateral dispersion of analytes and must be considered when designing effective separation protocols. Importantly, we found that favored separation conditions are achieved when the carrier electrolyte concentration is comparable to that of the analyte, balancing the need for sufficient electric field strength with minimal dispersion.

The positively charged MMBCD was selected as the chiral selector based on an extensive screening study using capillary electrophoresis. This analysis not only confirmed the preferential binding of RMA but also provided quantitative insight into the stability constants of the enantiomer-selector complexes. These findings were instrumental in guiding the design of the FFE experiments.

Although the enantiomeric ratio achieved in the FFE device was moderate, the separation was statistically significant and reproducible. The results confirm that continuous enantiomer separation is feasible. Further improvement could be achieved either by identifying a more selective chiral selectors through extensive screening or by refining operational parameters. More specific selectors could be designed and synthesized for a particular application, but this approach is time-consuming. In this study, we therefore limited ourselves to screening commercially available chiral selectors that provide at least limited separation capabilities at an acceptable cost.

We believe that our findings will contribute to the development of FFE methods and their broader application, particularly for the continuous production of enantiomers. In principle, FFE separation can be integrated as a module directly downstream of a chemical reactor or bioreactor to enable continuous enantiomer synthesis along with their separation. A modular reactor-FFE system could serve as a viable alternative to previously developed and tested systems such as bioreactor-membrane separator [35,55] or bioreactor-extraction unit [56,57] configurations.

Declaration of competing interest

The authors declare the following financial interests/personal relationships which may be considered as potential competing interests: Michal Pribyl reports financial support was provided by Czech Science Foundation. If there are other authors, they declare that they have no known competing financial interests or personal relationships that could have appeared to influence the work reported in this paper.

Acknowledgement

The authors thank the Czech Science Foundation for grant no. 24-11480S.

Data availability

Data will be made available on request.

References

[1] S.-J. Peng, Y.-Y. Zhu, C.-Y. Luo, P. Zhang, F.-Y. Wang, R.-X. Li, G.-Q. Lin, J.-G. Zhang, Chiral drugs: sources, absolute configuration identification,

pharmacological applications, and future research trends, LabMed Discovery 1 (1) (2024) 100008, https://doi.org/10.1016/j.lmd.2024.100008.
[2] G. Geisslinger, K.P. Stock, G.L. Bach, D. Loew, K. Brune, Pharmacological differences between R(−)-and S(+)-ibuprofen, Agents Actions 27 (3–4) (1989) 455–457, https://doi.org/10.1007/BF01972851.
[3] A. Jungbauer, P. Satzer, A. Duerauer, A. Azevedo, R. Aires-Barros, B. Nilsson, S. Farid, S. Goldrick, M. Ottens, M. Sponchioni, H. Marcelo Fernandez Lahore, Continuous downstream processing, Sep. Purif. Technol. 338 (2024) 126439, https://doi.org/10.1016/j.seppur.2024.126439.
[4] D. Sengar, V.V. Gopakumar, B.P. Chaudhari, V. Gajbhiye, Chapter 3 - Microfluidics in drug screening and drug delivery, in: D. Bodas, V. Gajbhiye (Eds.), Microfluidics-Aided Technologies, Academic Press, 2025, pp. 61–82, https://doi.org/10.1016/B978-0-323-95533-1.00007-2.
[5] A. Adamo, R.L. Beingessner, M. Behnam, J. Chen, T.F. Jamison, K.F. Jensen, J.-C. M. Monbaliu, A.S. Myerson, E.M. Revalor, D.R. Snead, T. Stelzer, N. Weeranoppanant, S.Y. Wong, P. Zhang, On-demand continuous-flow production of pharmaceuticals in a compact, reconfigurable system, Science 352 (6281) (2016) 61–67, https://doi.org/10.1126/science.aaf1337.
[6] Q. Zhu, Z. Cai, P. Zhou, X. Sun, J. Xu, Recent progress of membrane technology for chiral separation: a comprehensive review, Sep. Purif. Technol. 309 (2023) 123077, https://doi.org/10.1016/j.seppur.2022.123077.
[7] A.M. Stalcup, R.M.C. Sutton, P. Painuly, J.V. Rodrigo, S.R. Gratz, E.G. Yanes, Continuous free flow electrophoresis for preparative chiral separations of piperoxan using sulfated β-cyclodextrin, Analyst 125 (10) (2000) 1719–1724, https://doi.org/10.1039/b004347h.
[8] Z. Zhou, J.-H. Cheng, T.-S. Chung, T.A. Hatton, M. Toriida, K. Nishiura, S. Tamai, Enantiomeric resolution of tryptophan via stereoselective binding in an ion-exchange membrane partitioned free flow isoelectric focusing system, Chem. Eng. J. 174 (2) (2011) 522–529, https://doi.org/10.1016/j.cej.2011.08.083.
[9] P. Hoffmann, H. Wagner, G. Weber, M. Lanz, J. Caslavska, W. Thormann, Separation and purification of methadone enantiomers by continuous- and interval-flow electrophoresis, Anal. Chem. 71 (9) (1999) 1840–1850, https://doi.org/10.1021/ac981178v.
[10] R. Gajos, T.H. Dzido, Equipment and preliminary results for orthogonal high-pressure electrochromatography, Sep. Purif. Technol. 360 (2025) 131209, https://doi.org/10.1016/j.seppur.2024.131209.
[11] A.C. Johnson, M.T. Bowser, Micro free flow electrophoresis, Lab Chip 18 (1) (2018) 27–40, https://doi.org/10.1039/c7lc01105a.
[12] M. Přibyl, P. Izák, Z. Slouka, A mathematical model of a lateral electrochromatography device for continuous chiral separation, Sep. Purif. Technol. 282 (2022) 120033, https://doi.org/10.1016/j.seppur.2021.120033.
[13] A. Maruška, O. Kornyšova, Continuous beds (monoliths): stationary phases for liquid chromatography formed using the hydrophobic interaction-based phase separation mechanism, J. Biochem. Biophys. Methods 59 (1) (2004) 1–48, https://doi.org/10.1016/j.jbbm.2003.12.003.
[14] P. Glukhovskiy, G. Vigh, Analytical and preparative-scale isoelectric focusing separation of enantiomers, Anal. Chem. 71 (17) (1999) 3814–3820, https://doi.org/10.1021/ac9902749.
[15] E.M. van der Ent, P. van Hee, J.T.F. Keurentjes, K. van't Riet, A. van der Padt, Multistage electrodialysis for large-scale separation of racemic mixtures, J. Membr. Sci. 204 (1) (2002) 173–184, https://doi.org/10.1016/S0376-7388(02)00036-4.
[16] E. Schneiderman, S.R. Gratz, A.M. Stalcup, Optimization of preparative electrophoretic chiral separation of ritalin enantiomers, J. Pharm. Biomed. Anal. 27 (3) (2002) 639–650, https://doi.org/10.1016/S0731-7085(01)00572-6.
[17] P. Glukhovskiy, G. Vigh, Improved preparative-scale, continuous, free-flow electrophoretic separation of the enantiomers of terbutaline utilizing equal-but-opposite enantiomer mobilities, Electrophoresis 22 (13) (2001) 2639–2645, https://doi.org/10.1002/1522-2683(200108)22:13<2639::AID-ELPS2639>3.0.CO;2-T.
[18] C. Rougeot, J.E. Hein, Application of continuous preferential crystallization to efficiently access Enantiopure chemicals, Org. Process. Res. Dev. 19 (12) (2015) 1809–1819, https://doi.org/10.1021/acs.oprd.5b00141.
[19] J. Čížek, V. Jandová, P. Stanovský, Š. Hovorka, F. Yalcinkaya, M. Kohout, P. Izak, Chiral membranes prepared by ionic interactions between sulfobutylether-β-cyclodextrin and anion-exchange membranes, J. Membr. Sci. 717 (2025) 123592, https://doi.org/10.1016/j.memsci.2024.123592.
[20] R.-M. Nicoud, The amazing ability of continuous chromatography to adapt to a moving environment, Ind. Eng. Chem. Res. 53 (10) (2014) 3755–3765, https://doi.org/10.1021/ie5005866.
[21] D. Kohlheyer, J.C.T. Eijkel, A. van den Berg, R.B.M. Schasfoort, Miniaturizing free-flow electrophoresis – a critical review, Electrophoresis 29 (5) (2008) 977–993, https://doi.org/10.1002/elps.200700725.
[22] R.T. Turgeon, M.T. Bowser, Micro free-flow electrophoresis: theory and applications, Anal. Bioanal. Chem. 394 (1) (2009) 187–198, https://doi.org/10.1007/s00216-009-2656-5.
[23] C. Ooi, C.M. Earhart, C.E. Hughes, J.-R. Lee, D.J. Wong, R.J. Wilson, R. Rohatgi, S. X. Wang, Flow homogenization enables a massively parallel fluidic design for high-throughput and multiplexed cell isolation, Adv. Mater. Technol. 5 (5) (2020) 1900960, https://doi.org/10.1002/admt.201900960.
[24] Z. Zhu, L. Yang, Y. Yu, L. Zhang, S. Tao, Scale-up design of a fluorescent fluid photochemical microreactor by 3D printing, ACS Omega 5 (13) (2020) 7666–7674, https://doi.org/10.1021/acsomega.0c00511.
[25] S. Mahmud, S. Ramproshad, R. Deb, D. Dutta, A review of the zone broadening contributions in free-flow electrophoresis, Electrophoresis 44 (19–20) (2023) 1519–1538, https://doi.org/10.1002/elps.202300062.
[26] J. Lindner, D. Snita, M. Marek, Modelling of ionic systems with a narrow acid base boundary, Phys. Chem. Chem. Phys. 4 (8) (2002) 1348–1354, https://doi.org/10.1039/b109525k.
[27] M.A.K. Urtenov, E.V. Kirillova, N.M. Seidova, V.V. Nikonenko, Decoupling of the Nernst−Planck and Poisson equations. Application to a membrane system at overlimiting currents, J. Phys. Chem. B 111 (51) (2007) 14208–14222, https://doi.org/10.1021/jp073103d.
[28] J. Zhang, J. Yan, S. Li, B. Pang, C.-G. Guo, C.-X. Cao, X.-Q. Jin, Mathematical model and dynamic computer simulation on free flow zone electrophoresis, Analyst 138 (19) (2013) 5734–5744, https://doi.org/10.1039/C3AN00834G.
[29] S.N. Zheng, T. Hanai, T. Yonemoto, T. Tadaki, Separation of amino-acids by recycling free-flow electrophoresis, J. Chem. Eng. Jpn 25 (6) (1992) 686–691, https://doi.org/10.1252/jcej.25.686.
[30] R. Gajos, B. Polak, T.H. Dzido, Some theoretical considerations on preparative separation with orthogonal pressurised planar electrochromatography, J. Sep. Sci. 42 (4) (2019) 933–946, https://doi.org/10.1002/jssc.201800720.
[31] K. Yoo, J. Shim, J. Liu, P. Dutta, Mathematical and numerical model to study two-dimensional free flow isoelectric focusing, Biomicrofluidics 8 (3) (2014), https://doi.org/10.1063/1.4883575.
[32] T. Postler, Z. Slouka, M. Svoboda, M. Pribyl, D. Snita, Parametrical studies of electroosmotic transport characteristics in submicrometer channels, J. Colloid Interface Sci. 320 (1) (2008) 321–332, https://doi.org/10.1016/j.jcis.2007.10.056.
[33] P. Řezanka, K. Navrátilová, M. Řezanka, V. Král, D. Sýkora, Application of cyclodextrins in chiral capillary electrophoresis, Electrophoresis 35 (19) (2014) 2701–2721, https://doi.org/10.1002/elps.201400145.
[34] M. Rekharsky, Y. Inoue, Chiral recognition thermodynamics of β-Cyclodextrin: the thermodynamic origin of Enantioselectivity and the enthalpy−entropy compensation effect, J. Am. Chem. Soc. 122 (18) (2000) 4418–4435, https://doi.org/10.1021/ja9921118.
[35] L. Sauer, D. Kralik, Z. Slouka, M. Přibyl, Electric-field-assisted in situ separation of mandelic acid in an enzymatic milli-reactor improves the control of reaction conversion and enhances the enantiomeric ratio, Biochem. Eng. J. 205 (2024) 109280, https://doi.org/10.1016/j.bej.2024.109280.
[36] A.J. Grodzinsky, Fields, Forces, and Flows in Biological Systems, Garland Science, New York, 2011.
[37] COMSOL, Multiphysics Reference Manual 6.2, 2023.
[38] P.R. Amestoy, A. Buttari, J.-Y. L'Excellent, T. Mary, Performance and scalability of the block low-rank multifrontal factorization on multicore architectures, ACM Trans. Math. Softw. 45 (1) (2019), https://doi.org/10.1145/3242094. Article 2.
[39] P.R. Amestoy, I.S. Duff, J.-Y. L'Excellent, J. Koster, A fully asynchronous multifrontal solver using distributed dynamic scheduling, SIAM J. Matrix Anal. Applications 23 (1) (2001) 15–41, https://doi.org/10.1137/s0895479899358194.
[40] M. Erdős, M. Frangou, T.J.H. Vlugt, O.A. Moultos, Diffusivity of α-, β-, γ-cyclodextrin and the inclusion complex of β-cyclodextrin: ibuprofen in aqueous solutions; A molecular dynamics simulation study, Fluid Phase Equilib. 528 (2021) 112842, https://doi.org/10.1016/j.fluid.2020.112842.
[41] G. Calderó, M.J. García-Celma, C. Solans, R. Pons, Effect of pH on mandelic acid diffusion in water in oil highly concentrated emulsions (gel-emulsions), Langmuir 16 (4) (2000) 1668–1674, https://doi.org/10.1021/la990971w.
[42] J.F.G. Reis, E.N. Lightfoot, H.-L. Lee, Concentration profiles in free-flow electrophoresis, AICHE J. 20 (2) (1974) 362–368, https://doi.org/10.1002/aic.690200224.
[43] Y. Tanaka, Concentration polarization in ion-exchange membrane electrodialysis: the events arising in an unforced flowing solution in a desalting cell, J. Membr. Sci. 244 (1) (2004) 1–16, https://doi.org/10.1016/j.memsci.2004.02.041.
[44] J.-H. Choi, J.-S. Park, S.-H. Moon, Direct measurement of concentration distribution within the boundary layer of an ion-exchange membrane, J. Colloid Interface Sci. 251 (2) (2002) 311–317, https://doi.org/10.1006/jcis.2002.8407.
[45] P. Kovář, D. Tichý, Z. Slouka, Effect of channel geometry on ion-concentration polarization-based preconcentration and desalination, Biomicrofluidics 13 (6) (2019), https://doi.org/10.1063/1.5124787.
[46] V. Nikonenko, M. Urtenov, S. Mareev, G. Pourcelly, Mathematical modeling of the effect of water splitting on ion transfer in the depleted diffusion layer near an ion-exchange membrane, Membranes 10 (2) (2020) 22, https://doi.org/10.3390/membranes10020022.
[47] J. de Valença, M. Jõgi, R.M. Wagterveld, E. Karatay, J.A. Wood, R.G. H. Lammertink, Confined electroconvective vortices at structured ion exchange membranes, Langmuir 34 (7) (2018) 2455–2463, https://doi.org/10.1021/acs.langmuir.7b04135.
[48] Y. Green, S. Shloush, G. Yossifon, Effect of geometry on concentration polarization in realistic heterogeneous permselective systems, Phys. Rev. E 89 (4) (2014) 043015, https://doi.org/10.1103/PhysRevE.89.043015.
[49] T. Belloň, P. Polezhaev, L. Vobecká, M. Svoboda, Z. Slouka, Experimental observation of phenomena developing on ion-exchange systems during current-voltage curve measurement, J. Membr. Sci. 572 (2019) 607–618, https://doi.org/10.1016/j.memsci.2018.11.037.
[50] M. Pribyl, D. Snita, M. Marek, Nonlinear phenomena and qualitative evaluation of risk of clogging in a capillary microreactor under, imposed electric field, Chem. Eng. J. 105 (3) (2005) 99–109, https://doi.org/10.1016/j.cej.2004.10.003.
[51] R. Ratih, H. Wätzig, M. Stein, S. El Deeb, Investigation of the enantioselective interaction between selected drug enantiomers and human serum albumin by mobility shift-affinity capillary electrophoresis, J. Sep. Sci. 43 (20) (2020) 3960–3968, https://doi.org/10.1002/jssc.202000372.
[52] P. Řezanka, K. Řezanková, H. Sedláčková, J. Mašek, L. Rokosová, M. Bláhová, M. Řezanka, J. Jindřich, D. Sýkora, V. Král, Influence of substituent position and

cavity size of the regioisomers of monocarboxymethyl-α-, β-, and γ-cyclodextrins on the apparent stability constants of their complexes with both enantiomers of Tröger's base, J. Sep. Sci. 39 (5) (2016) 980–985, https://doi.org/10.1002/jssc.201500845.

[53] P.A. Levkin, N.M. Maier, V. Schurig, W. Lindner, Strong detrimental effect of a minute enantiomeric impurity of a chiral selector on the Enantioselectivity factor, Angew. Chem. Int. Ed. 49 (42) (2010) 7742–7744, https://doi.org/10.1002/anie.201002215.

[54] J. Znaleziona, I. Fejős, J. Ševčík, M. Douša, S. Béni, V. Maier, Enantiomeric separation of tapentadol by capillary electrophoresis—study of chiral selectivity manipulation by various types of cyclodextrins, J. Pharm. Biomed. Anal. 105 (2015) 10–16, https://doi.org/10.1016/j.jpba.2014.11.027.

[55] D. Kralik, A. Kovárová, L. Vobecká, P. Hasal, Z. Slouka, M. Pribyl, Continuous flow synthesis and separation of mandelic acid enantiomers in a modular microfluidic system, Sep. Purif. Technol. 309 (2023), https://doi.org/10.1016/j.seppur.2022.123009.

[56] L. Sauer, M. Pribyl, Enzyme synthesis and continuous flow separation of (R)-1-phenylethanol in a modular microfluidic system, Sep. Purif. Technol. 360 (2025), https://doi.org/10.1016/j.seppur.2024.131041.

[57] L. Vobecká, L. Tichá, A. Atanasova, Z. Slouka, P. Hasal, M. Přibyl, Enzyme synthesis of cephalexin in continuous-flow microfluidic device in ATPS environment, Chem. Eng. J. 396 (2020) 125236, https://doi.org/10.1016/j.cej.2020.125236.